NASA TN D-988

TECHNICAL NOTE

D-988

FREE-FLIGHT INVESTIGATION OF HEAT TRANSFER TO AN UNSWEPT CYLINDER SUBJECTED TO AN INCIDENT SHOCK AND FLOW INTERFERENCE FROM AN UPSTREAM BODY AT MACH NUMBERS UP TO 5.50

By Howard S. Carter and Robert E. Carr

Langley Research Center
Langley Air Force Base, Va.

NATIONAL AERONAUTICS AND SPACE ADMINISTRATION

WASHINGTON October 1961

NATIONAL AERONAUTICS AND SPACE ADMINISTRATION

TECHNICAL NOTE D-988

FREE-FLIGHT INVESTIGATION OF HEAT TRANSFER TO AN UNSWEPT CYLINDER SUBJECTED TO AN INCIDENT SHOCK AND FLOW INTERFERENCE FROM AN UPSTREAM BODY AT MACH NUMBERS UP TO 5.50

By Howard S. Carter and Robert E. Carr

SUMMARY

Heat-transfer rates have been measured in free flight along the stagnation line of an unswept cylinder mounted transversely on an axial cylinder so that the shock wave from the hemispherical nose of the axial cylinder intersected the bow shock of the unswept transverse cylinder. Data were obtained at Mach numbers from 2.53 to 5.50 and at Reynolds numbers based on the transverse cylinder diameter from 1.00×10^6 to 1.87×10^6.

Shadowgraph pictures made in a wind tunnel showed that the flow field was influenced by boundary-layer separation on the axial cylinder and by end effects on the transverse cylinder as well as by the intersecting shocks. Under these conditions, the measured heat-transfer rates had inconsistent variations both in magnitude and distribution which precluded separating the effects of these disturbances. The general magnitude of the measured heating rates at Mach numbers up to 3 was from 0.1 to 0.5 of the theoretical laminar heating rates along the stagnation line for an infinite unswept cylinder in undisturbed flow. At Mach numbers above 4 the measured heating rates were from 1.5 to 2 times the theoretical rates.

INTRODUCTION

Along with the increasing speed of high-performance aircraft has come, necessarily, an increasing emphasis on the problem of aerodynamic

heating. In recent years research has been devoted to determining the heat transfer to blunt bodies, such as cylinders, and wing leading edges subjected to uniform high-speed flow in order to obtain information useful in design. The problem of determining the heat transfer to wings or bodies subjected to a nonuniform flow field, as in the case where a wing or body is subjected to shocks and other disturbances originating from another body, has more recently come under scrutiny with the advent of such vehicles as the X-15 and Dyna-Soar.

To investigate the influence of a nonuniform flow field on heating rate to an unswept cylinder, a two-stage rocket model system was designed and launched from the NASA Wallops Station. The cruciform-shaped test configuration, which was mounted on the nose of the second stage, consisted of two cylinders having nearly equal diameters and instrumented to measure skin temperatures along the stagnation line of the transverse cylinder. The shock wave from the hemispherical nose of the axial cylinder impinged on the bow shock of the unswept transverse cylinder. Also, the upstream axial cylinder and its boundary layer caused other disturbances in the flow on the transverse cylinder. Aerodynamic heating rates were obtained along the stagnation line of the unswept transverse cylinder for Mach numbers up to 5.50 and Reynolds numbers based on the transverse cylinder diameter from 1.00×10^6 to 1.87×10^6. Results from this test and some concluding remarks are presented herein.

L 8 7 9

SYMBOLS

D	diameter of transverse cylinder, 0.0625 ft
d	diameter of hemispherical-tipped axial cylinder, 0.0734 ft
h	measured heat-transfer coefficient, Btu/sec-ft^2-$^\circ$R
h_L	theoretical heat-transfer coefficient for laminar flow, Btu/ft^2-sec-$^\circ$R
k	coefficient of thermal conductivity, Btu-ft/sec-ft^2-$^\circ$R
l	length along stagnation line between thermocouple stations, ft
M	Mach number
p	pressure, lb/sq ft
Q	spanwise conduction at station n, Btu/sec-ft^2

q	heating rate, Btu/sec-ft^2
R_∞	free-stream Reynolds number per foot
R_D	free-stream Reynolds number based on transverse cylinder diameter
r'	radius of transverse cylinder, ft
T	temperature, ^oR
TC	abbreviation for thermocouple in figures 3 and 10
t	time, sec
V	velocity, ft/sec
x	distance along transverse cylinder from model center line, ft
y	distance along axial cylinder from hemispherical nose tip, ft
θ	circumferential angle, radian
ρ	density, slugs/cu ft
τ	skin thickness, ft

Subscripts:

i	inner surface
n	nth term in numerical series (1, 2, 3, . . ., n)
o	outer surface
t	stagnation
w	wall
∞	free stream

MODEL, INSTRUMENTATION, AND TEST

Model

The model consisted of a flare-stabilized JATO, 1.52-KS-33,550, SM19 (Recruit) rocket motor with the test nose and instrument section mounted on the forward end of the motor. The test nose which was a cruciform configuration consisted of a hemispherical-tipped cylinder to serve as a shock producer, and a transverse cylinder with zero sweep on which the heat-transfer measurements were made. The transverse cylinder was located so that at high speeds the shock from the hemispherical tip would intersect the shock wave of the transverse cylinder. Photographs of the model and the test nose are shown in figures 1 and 2, respectively. The shock producing tip of the test nose and the transverse cylinder were made of Inconel. The remaining part of the cruciform test nose was made of mild carbon steel (SAE 1018). In order to obtain a fast temperature response through the wall of the transverse cylinder, a nominal wall thickness of 0.032 inch was used. As predicted by use of reference 1, this thickness would be sufficient to withstand the heating through the peak Mach number of the test. This prediction did not include effects due to a nonuniform flow field.

Instrumentation

The model was equipped with a telemetering system which transmitted the data to a ground receiving station. Three channels were used to transmit the accelerations (longitudinal, transverse, and normal) experienced by the model, and two channels were used to transmit the temperatures measured along the cylinder semispan at the thermocouple locations. Figure 3 shows the seven evenly spaced thermocouples mounted along the stagnation line on the inside surface of the transverse cylinder. Temperature data from thermocouples 1, 2, 3, 5, 6, and 7 were commutated and transmitted on one of these temperature channels so that each thermocouple recorded about every 0.1 second. Temperature data from thermocouple 4 were transmitted continuously on the other temperature channel. The maximum probable error of the temperature measurement was ±2 percent of the calibrated full-scale value, or, in this case, ±40°.

In addition to the internally carried instrumentation, the model was tracked by a CW Doppler velocimeter to provide the velocity-time history, and by two different radar sets, a NASA modified SCR-584 tracking radar and an AN/FPS-16 radar set. Each provided flight-path data for the test. Atmospheric and wind conditions were determined by means of a radiosonde launched near the time of flight and tracked by a Rawin set AN/GMD-1A.

Test

The model was launched at an elevation angle of 60°. The booster, a fin-stabilized M5 JATO rocket motor (Nike), accelerated the model to a Mach number of about 3.0. A picture of the model and booster on the launcher is shown in figure 4. After a short coast period, the sustainer rocket ignited, effected separation from the spent booster, and accelerated the model to its peak Mach number of 7.4.

At a Mach number of 5.91, which occurred 1.14 seconds after ignition of the sustainer, the telemeter signal was lost. However, radar tracking indicated that the model continued accelerating along its anticipated flight path until after sustainer burnout. The telemetered data showed that at the time of signal failure the temperatures on the stagnation line of the transverse cylinder were rising very rapidly and were approaching the structural thermal limit of Inconel. (It may be noted that if boundary-layer transition occurred on the transverse cylinder, the stagnation line would not necessarily be the hottest location.)

At sustainer ignition the model experienced an oscillation in pitch which had damped to essentially zero degrees at the time of signal failure 1.14 seconds later. The high temperatures and air loads encountered probably caused a breakup of the model nose and loss of telemeter signal without completely destroying the vehicle.

Heating data presented in this report are for the time of flight up to 5.34 seconds ($M_\infty = 5.50$), during which time telemeter signals were received. This Mach number was reached at an altitude of 10,500 feet with a corresponding Reynolds number of 1.87×10^6 based on the transverse cylinder diameter.

DATA REDUCTION

Trajectory Data

Time histories of model velocity, Mach number, Reynolds number per foot, and altitude are presented in figure 5. Variations of the free-stream air properties (temperature, density, and pressure) with flight time are given in figure 6. The model velocity was obtained by integration of the longitudinal acceleration up to the time of telemeter failure and thereafter from the CW Doppler velocimeter data. The other data of figures 5 and 6 were obtained from ground radar and radiosonde measurements.

Heating Rates

Faired curves showing the variation of skin temperatures with time are plotted in figure 7. The curves for different stations end at different times because the thermocouples, except for the one at station 4, were commutated on a single channel. The faired curves of measured inside wall temperature were used to compute the outside surface temperature. The outside surface temperatures were then used to compute one-dimensional heating rates. The computational methods used were those of reference 2, which considers a thermally thick wall without curvature and with no heat flow parallel to the wall and no plate curvature. Effect of wall curvature was not included but would increase the heating rates less than 5 percent. Faired curves of the experimental one-dimensional heating rates for two representative stations are shown in figure 8.

The aerodynamic heat-transfer rate at a measurement station is considered to be equal to the one-dimensional heating rate plus the rates of heat loss at the station due to conduction and radiation. Sample computations of radiation showed it to be always less than 2 percent of the one-dimensional heating rate and it was therefore disregarded. Likewise, conduction along the skin normal to the stagnation line was disregarded since estimates showed it to be always less than $3\frac{1}{2}$ percent of the one-dimensional heating rates. The estimates were made by use of temperature distributions derived from the laminar heat-transfer distributions on an unswept cylinder in reference 3. The rate of heat accumulation at a station due to spanwise conduction along the stagnation line was computed by a finite-difference method by use of the measured temperatures and the following equation:

$$Q = \frac{k\left(T_{n-1} - T_n\right)\tau(r'd\theta)}{l\,l(r'd\theta)} - \frac{k\left(T_n - T_{n+1}\right)\tau(r'd\theta)}{l\,l(r'd\theta)}$$

$$= \frac{k\tau}{l^2}\left(T_{n-1} - T_n\right) - \left(T_n - T_{n+1}\right)$$

The one-dimensional heating rates were corrected by this spanwise conduction term to determine aerodynamic heating rate.

RESULTS AND DISCUSSION

Shock Position

An estimation was made of the location of the intersection of the shock wave from the hemispherical nose and the bow shock of the transverse cylinder since it was expected that this location would have a strong influence on the distribution of heating along the transverse cylinder. In estimating the position of these shocks, use was made of unpublished results from tests of a similar nose configuration made in the preflight jet at NASA Wallops Station at a Mach number of 2 and in the Langley Unitary Plan wind tunnel at Mach numbers of 2.65 and 4.44. In those tests the transverse cylinder was about 2 diameters longer in span than in the present flight test. Figure 9 presents a shadowgraph from each of these tests. In each, a dark line extends from the intersection of the two strong shocks towards the surface of the transverse cylinder. Since the flow in this region near the stagnation line of the transverse cylinder is subsonic, this dark line does not indicate a shock wave but may be a slip plane or the three-dimensional photographic effects of the shock intersection.

Separation of the boundary layer on the axial cylinder in front of the transverse cylinder is also apparent in the shadowgraphs. The presence of spanwise flow and the general complexity of the flow field around the configuration are indicated by the spanwise curvature of the bow shock outboard of the shock intersection and the irregularity of the shock inboard of the intersection.

Measurements of the shock shape from these shadowgraphs are shown in figure 10 along with shock shapes for several Mach numbers which were predicted by the method of reference 4. A comparison of the measured shock shapes shows very close agreement with the predicted shapes. The approximate spanwise location of the intersection of the nose shock wave and the bow shock wave is shown in figure 11 as a function of Mach number. The location is given in terms of either the nose diameter or the diameter of the transverse cylinder. Both plots are included since the shape of the nose shock (and thus the location of the intersection) is dependent on nose diameter; whereas, in subsequent figures spanwise location on the transverse cylinder is presented in terms of the diameter of the transverse cylinder.

Heat Transfer

The spanwise distributions of the experimental heating rates on the transverse cylinder are presented in figure 12 for several times during the flight test over the Mach number range from 2.25 to 5.50. Both the

one-dimensional and the aerodynamic heating rates are shown, their difference being the correction for spanwise conduction. The outside wall temperatures at the thermocouple locations are shown, connected by straight lines which indicate the spanwise temperature distributions assumed in the computation of the conduction corrections. Also shown on each distribution is the spanwise location of the intersection of the nose shock and the bow shock of the transverse cylinder as determined from figure 11.

The theoretical laminar heating-rate distributions were determined from the following relation:

$$q = h_L(T_t - T_{wo})$$

with the use of the plotted experimental values of T_{wo} and theoretical values of h_L for the stagnation line of an unyawed infinite cylinder (i.e., no variation in h_L with spanwise location) as determined from equation (B5) of reference 3. This theory was shown in reference 3 to agree within 8 percent with wind-tunnel results at $M = 4.15$ over the Reynolds number range of the present test.

The theoretical turbulent distributions shown in figure 12 were determined by use of theory presented in reference 5 and are for a location 5° chordwise from the stagnation line on an unyawed infinite cylinder at the flight test conditions. They are shown primarily for comparison with the theoretical laminar rates to indicate the predicted increase in heating rate for turbulent flow near the stagnation line. According to the theory of reference 5, turbulent rates for a given chordwise location are a multiple of the laminar rates for that location, with the multiplier being a function only of the local Reynolds number based on surface length from the stagnation line. Local Reynolds numbers at a 5° location for the flight conditions were determined by use of Newtonian pressure distribution and the compressible-flow relations of reference 6. An error of about 1 percent was introduced by basing the theoretical turbulent rates on laminar theory for the stagnation line rather than on laminar theory for the 5° location.

The shadowgraph pictures of figure 9 show that the flow field was influenced by boundary-layer separation and by end effects from the transverse cylinder as well as by the intersecting shocks. (To determine the effect of these intersecting shocks was the original intention of the test.) Figure 12 shows that under these conditions, the measured heat-transfer rates had inconsistent variations both in magnitude and distribution which precluded separating the effects of these flow disturbances. For example, no consistent effect of the shock intersection on heat transfer was apparent.

The relatively high heating rates at the two inboard stations at times prior to 3.66 seconds, which caused the temperatures at these two stations to rise rapidly (see fig. 7(a)), are apparently not associated with Mach number and Reynolds number since they persisted only part way through the period of relatively constant flight conditions between 3.0 and 4.5 seconds. The heating rates at the outboard station are, except at the two highest Mach numbers, higher than at the neighboring inboard stations; this may be due to end effects on the transverse cylinder.

L 8 7 9 At Mach numbers up to 3.23 (figs. 12(a) to 12(l)) the experimental heating rates were generally much less than laminar theory for an infinite cylinder, except at the two inboard stations where the previously noted high heating rates were sometimes as high as the turbulent theory for the 5° chordwise location. At Mach numbers above 3.23 the measured rates generally exceeded the laminar theory at all measurement stations.

For convenient comparison of the experimental data with the laminar infinite-cylinder theory, the experimental heating rates divided by the corresponding laminar theoretical rates, as obtained from figure 12, are plotted in figure 13. (Note that the measured heating rate divided by the theoretical laminar heating rate is identical to the measured heat-transfer coefficient divided by the theoretical laminar heat-transfer coefficient since the experimental values of $T_t - T_{wo}$ were used to compute the theoretical laminar heating rate.) Except at the two inboard stations, the general level of h/h_L along the transverse cylinder was between 0.1 and 0.5 at Mach numbers up to 3.23. As the Mach number increased from 3.23 to 5.50, the general level of h/h_L increased to values between 1.5 and 2.0, with considerable spanwise variation of the ratio in most cases.

At times from 3.84 seconds to 5.16 seconds the magnitude of h/h_L is high near the shock-intersection location relative to values at neighboring locations. However, this condition is not evident after 5.16 seconds, nor before 3.84 seconds, even though Mach number and Reynolds number were approximately constant from about 3.0 seconds to 4.5 seconds.

Results of the present free-flight test show a considerably lower level of heat transfer along the stagnation line of an unswept cylinder in a flow field disturbed by an upstream body than did data obtained recently in the Langley Unitary Plan wind tunnel. (See ref. 7.) Also, the present flight test did not show an increase in heat transfer near the shock intersection as did the wind-tunnel tests. There were some differences between the flight test and the wind-tunnel tests, both in geometry and test conditions, which precluded a good comparison of the results.

CONCLUDING REMARKS

Heat-transfer rates have been measured in free flight along the stagnation line of an unswept cylinder mounted transversely on an axial cylinder so that the shock wave from the hemispherical nose of the axial cylinder intersected the bow shock of the unswept transverse cylinder. Data were obtained at Mach numbers from 2.53 to 5.50 and Reynolds numbers based on the transverse-cylinder diameter from 1.00×10^6 to 1.87×10^6.

Shadowgraph pictures made in a wind tunnel showed that the flow field was influenced by boundary-layer separation on the axial cylinder and by end effects on the transverse cylinder as well as by the intersecting shocks. Under these conditions, the measured heat-transfer rates had inconsistent variations both in magnitude and distribution which precluded separating the effects of these disturbances. The general magnitude of the measured heating rates at Mach numbers up to 3 was from 0.1 to 0.5 of theoretical laminar heating rates along the stagnation line for an infinite unswept cylinder in undisturbed flow. At Mach numbers above 4 the general magnitude of the measured heating rates was from 1.5 to 2 times the theoretical rates.

L 8 7 9

Langley Research Center,
National Aeronautics and Space Administration,
Langley Field, Va., June 22, 1961.

REFERENCES

1. Goodwin, Glen: Heat-Transfer Characteristics of Blunt Two- and Three-Dimensional Bodies at Supersonic Speeds. NACA RM A55L13a, 1956.

2. Hill, P. R.: A Method of Computing the Transit Temperature of Thick Walls From Arbitrary Variation of Adiabatic-Wall Temperature and Heat-Transfer Coefficient. NACA Rep. 1372, 1958. (Supersedes NACA TN 4105.)

3. Beckwith, Ivan E., and Gallagher, James J.: Local Heat Transfer and Recovery Temperatures on a Yawed Cylinder at a Mach Number of 4.15 and High Reynolds Numbers. NASA TR R-104, 1961. (Supersedes NASA MEMO 2-27-59L.)

4. Love, Eugene S.: A Reexamination of the Use of Simple Concepts for Predicting the Shape and Location of Detached Shock Waves. NACA TN 4170, 1957.

5. Van Driest, E. R.: On Skin Friction and Heat Transfer Near the Stagnation Point. Rep. No. AL-2267, North American Aviation, Inc., Mar. 1, 1956.

6. Ames Research Staff: Equations, Tables, and Charts for Compressible Flow. NACA Rep. 1135, 1953. (Supersedes NACA TN 1428.)

7. Newlander, Robert A.: Effect of Shock Impingement on the Distribution of Heat-Transfer Coefficients on a Right Circular Cylinder at Mach Numbers of 2.65, 3.51, and 4.44. NASA TN D-642, 1961.

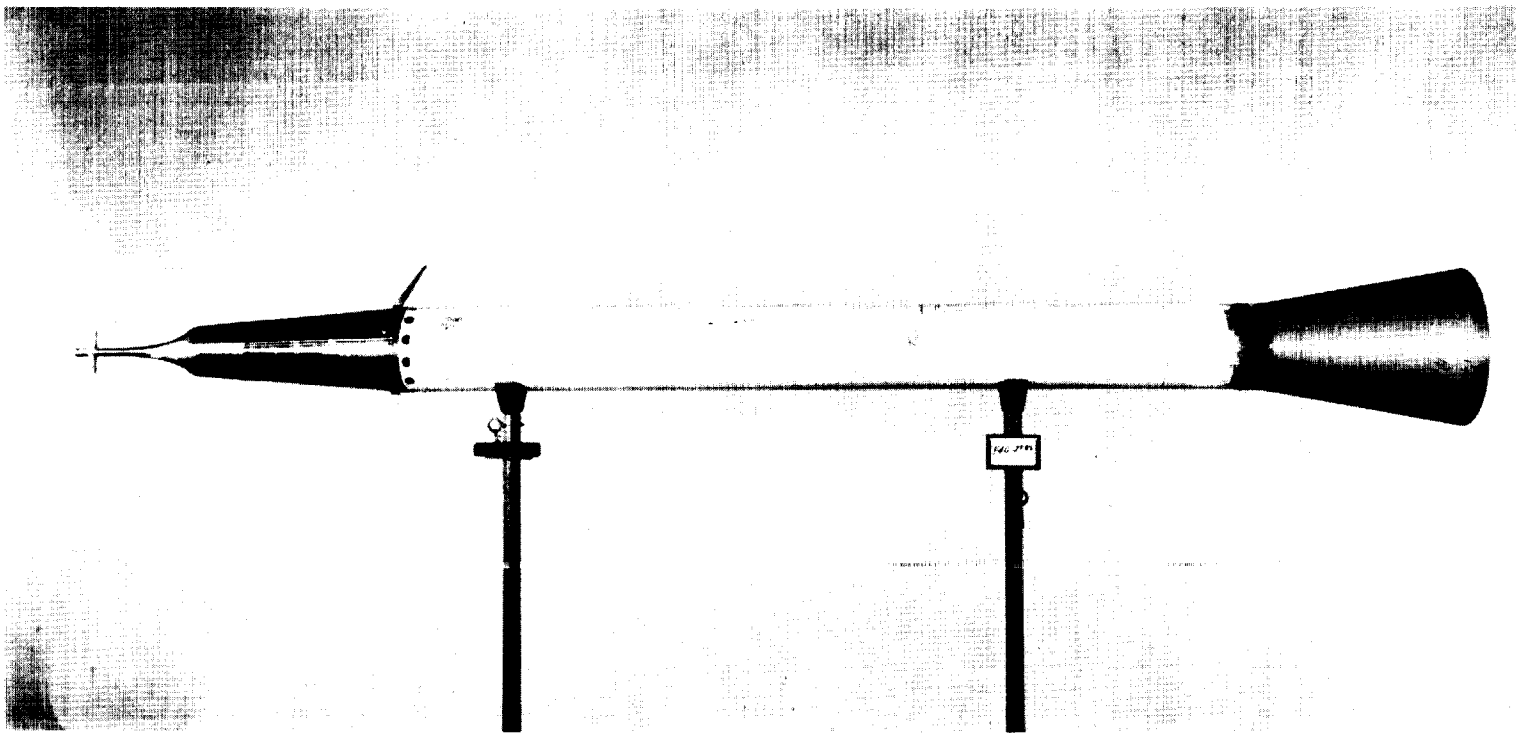

Figure 1.- Photograph of model. L-58-1099a

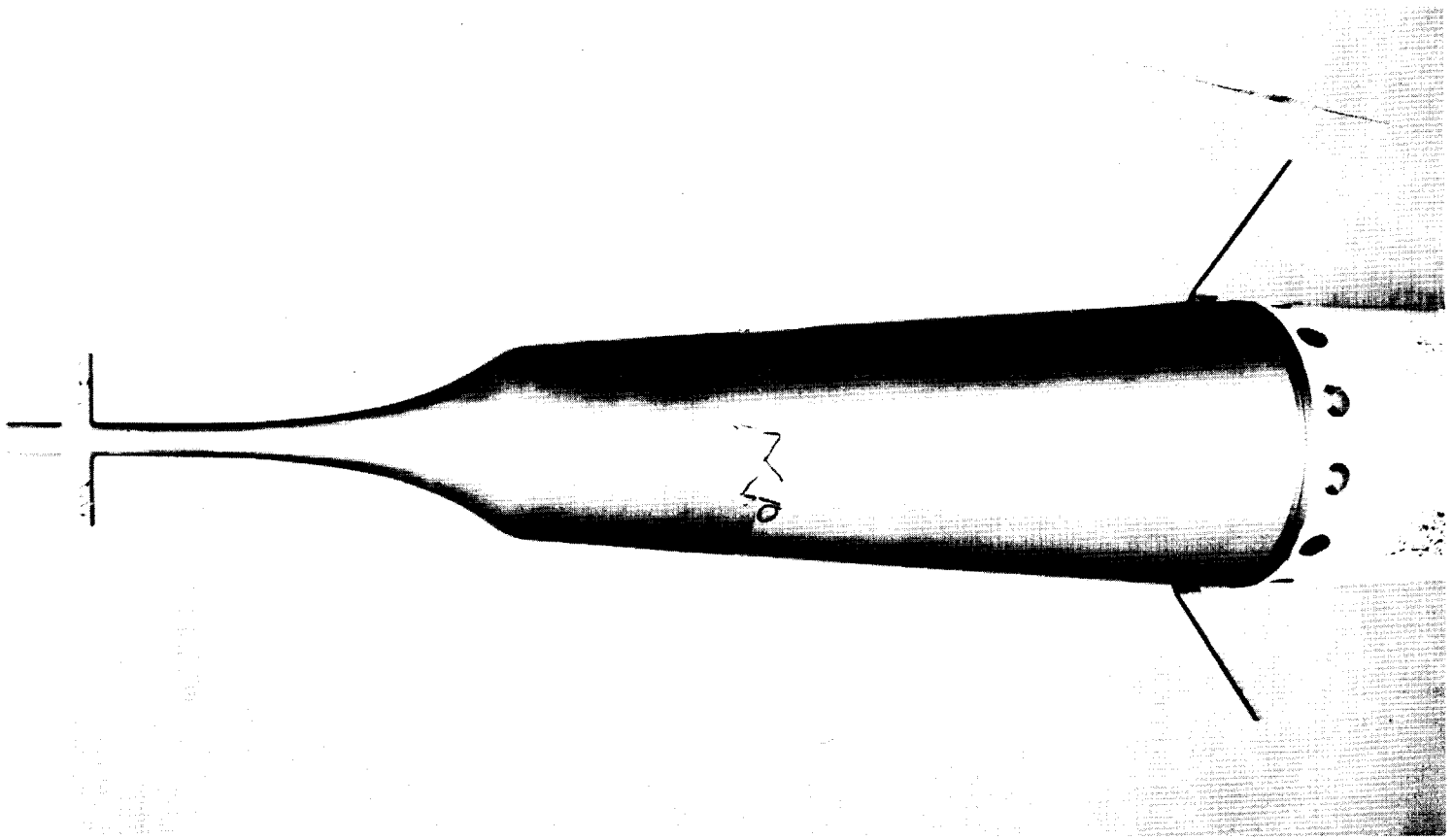

Figure 2.- Photograph of test nose. L-58-1100a

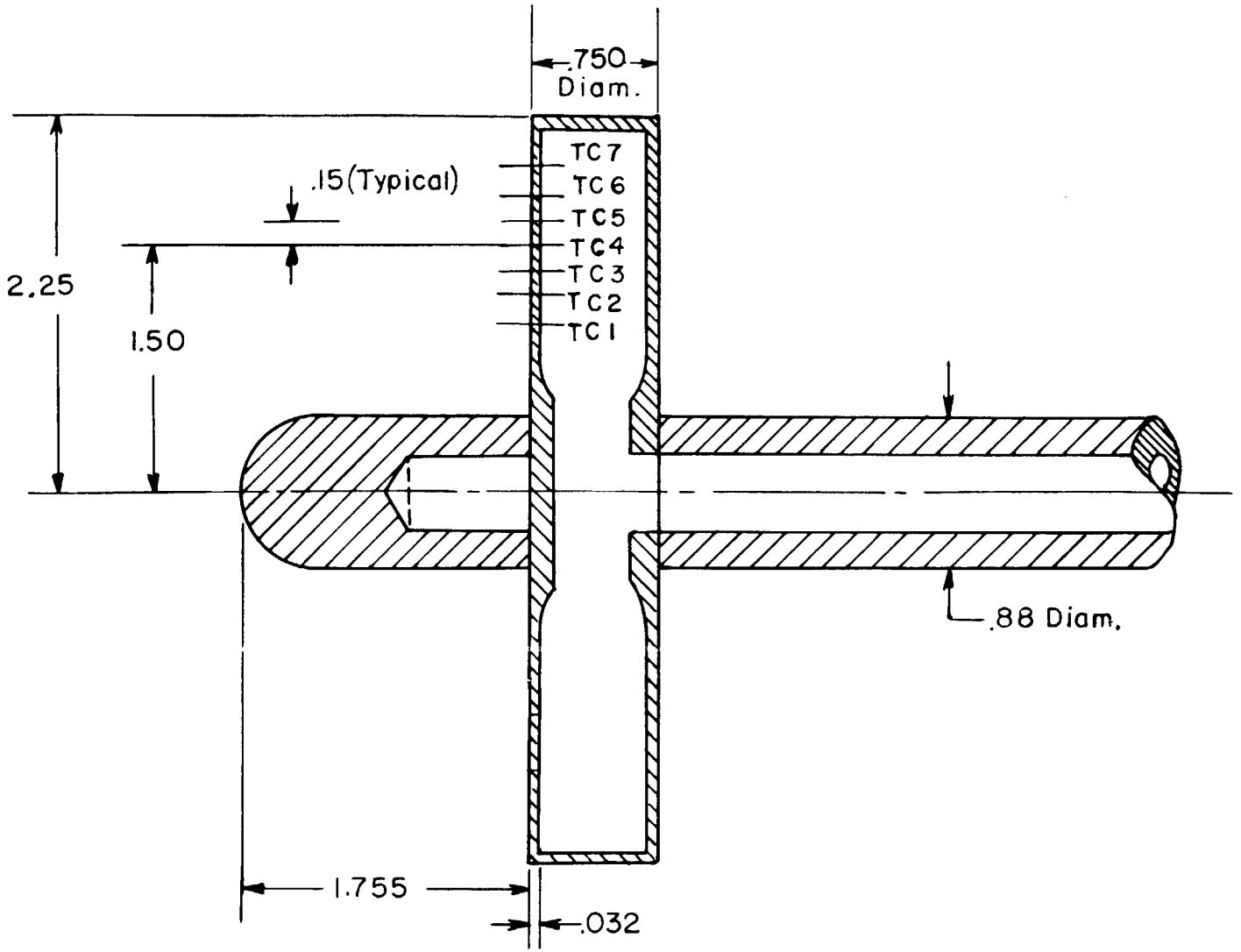

Figure 3.- Sketch of the test nose. All dimensions are in inches.

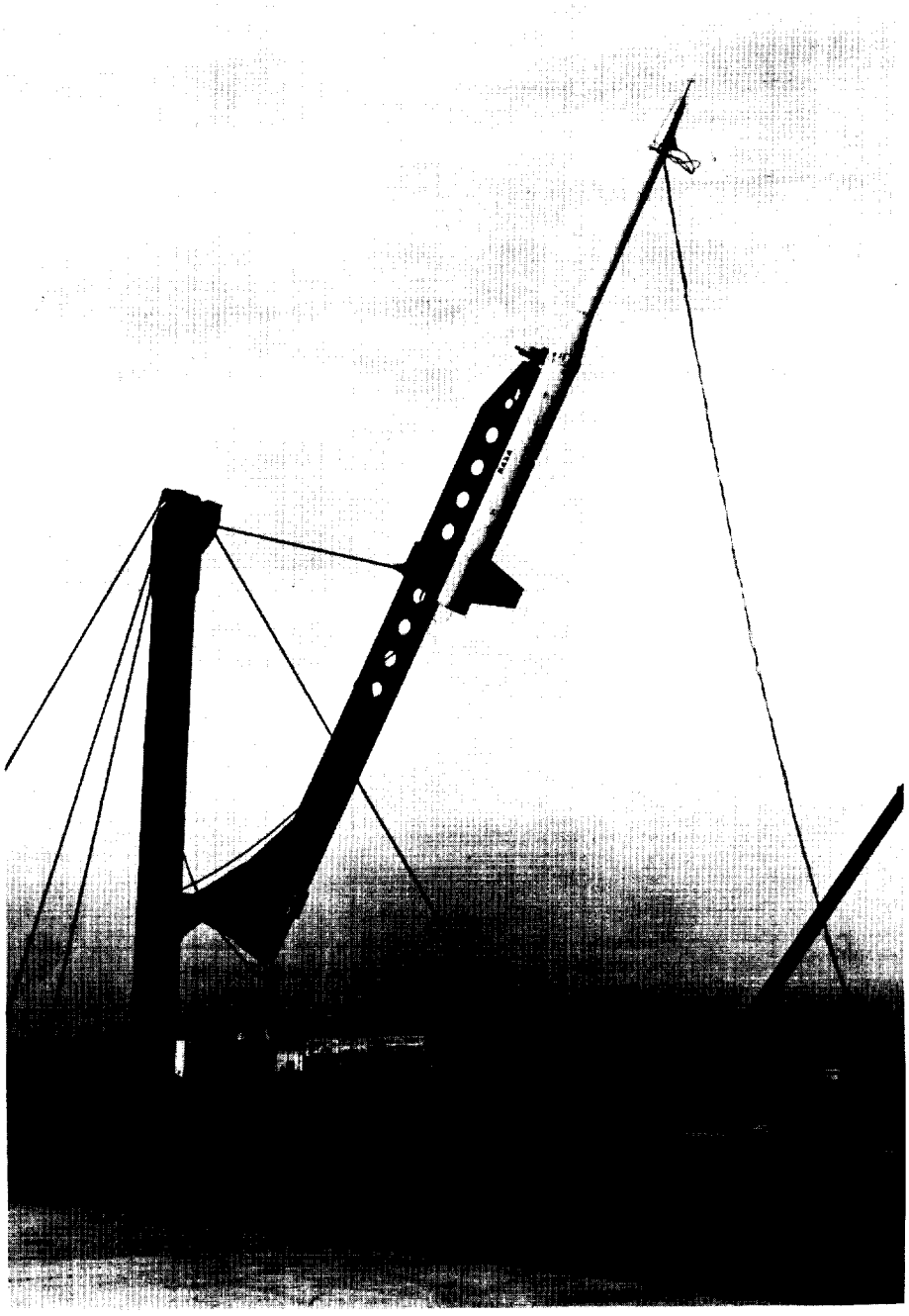

L-59-416

Figure 4.- Photograph of model-booster combination on launcher.

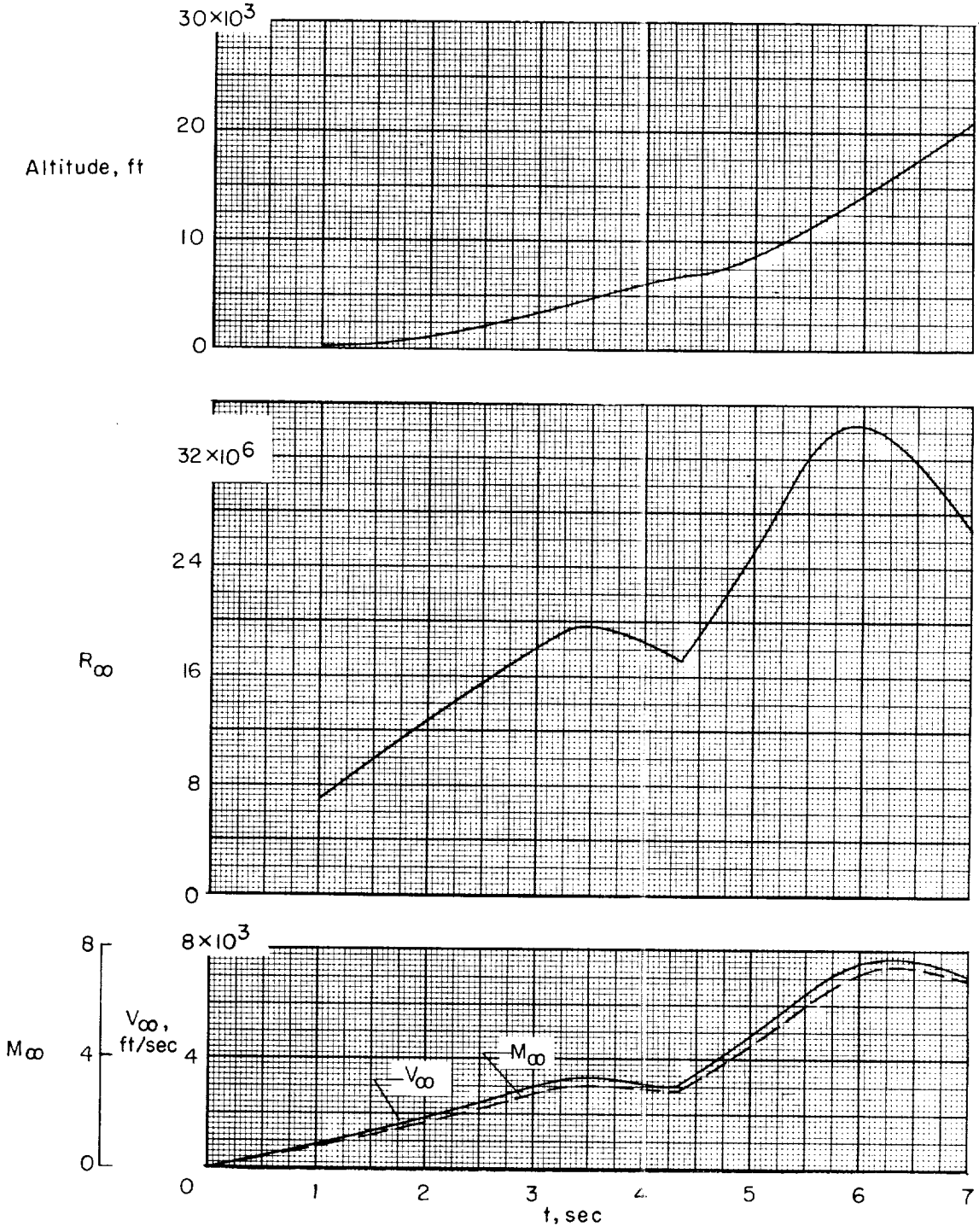

Figure 5.- Variation of model velocity, Mach number, Reynolds number per foot, and altitude with flight time.

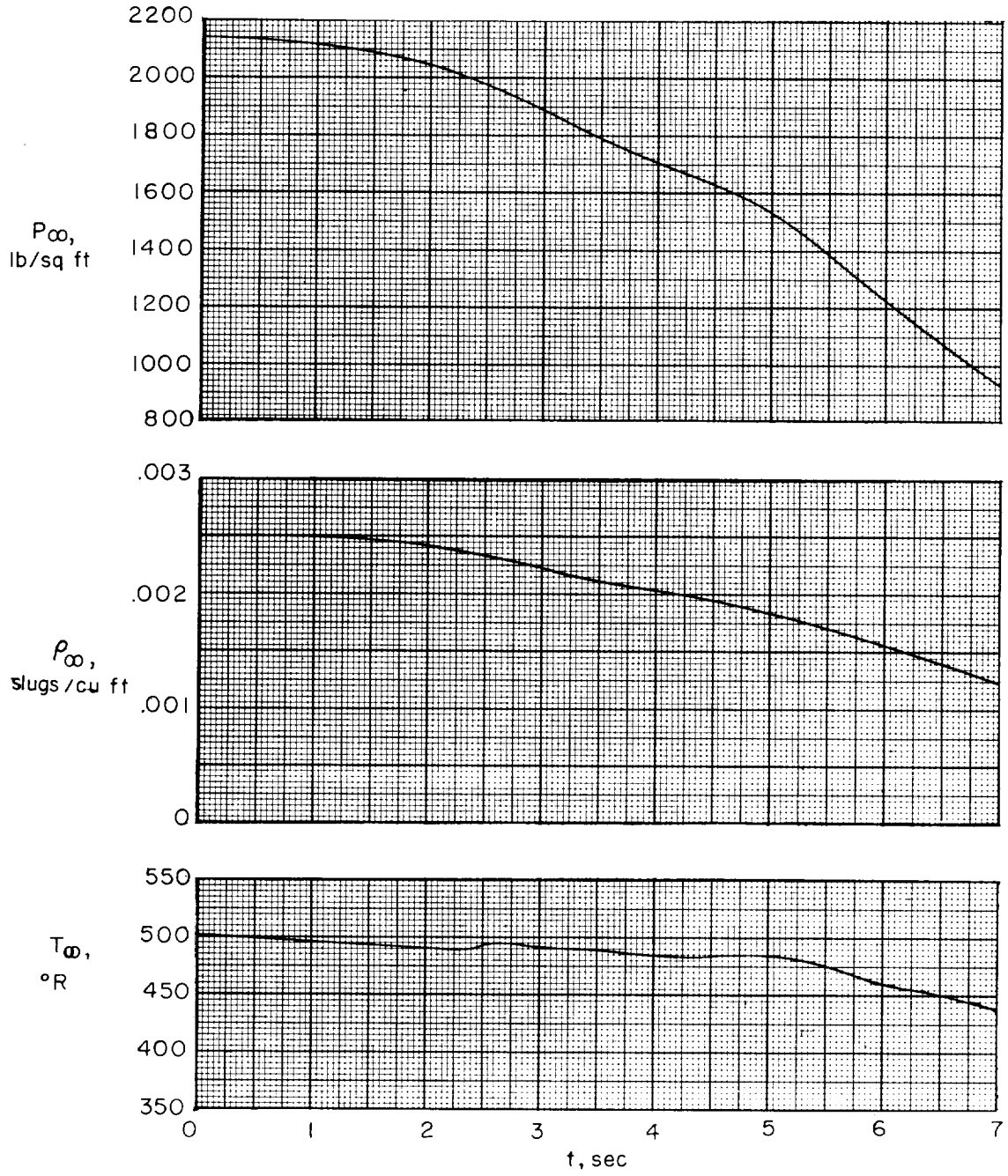

Figure 6.- Variation of free-stream density, pressure, and temperature with flight time.

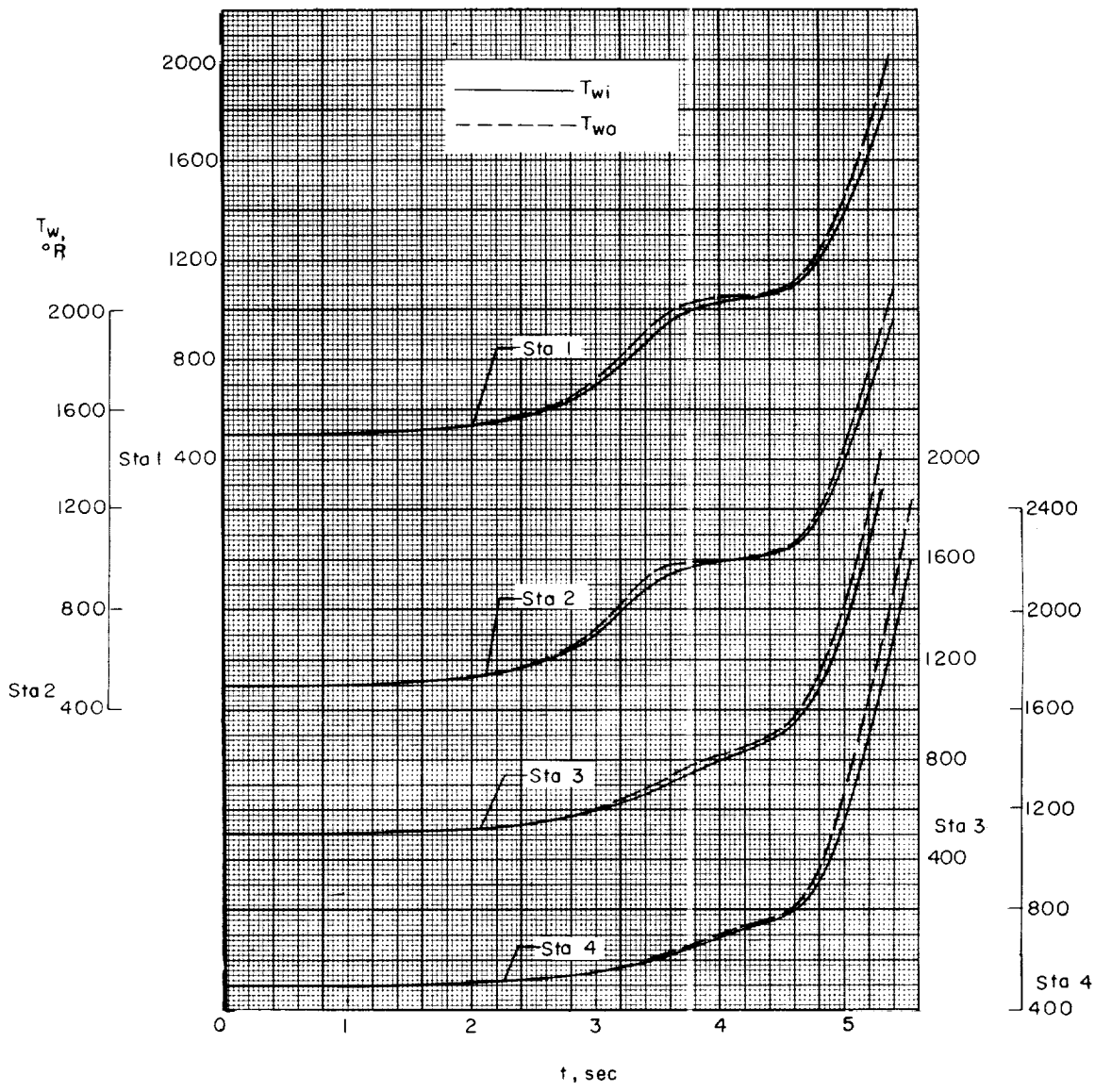

(a) Stations 1, 2, 3, and 4.

Figure 7.- Variation of skin temperature with flight time.

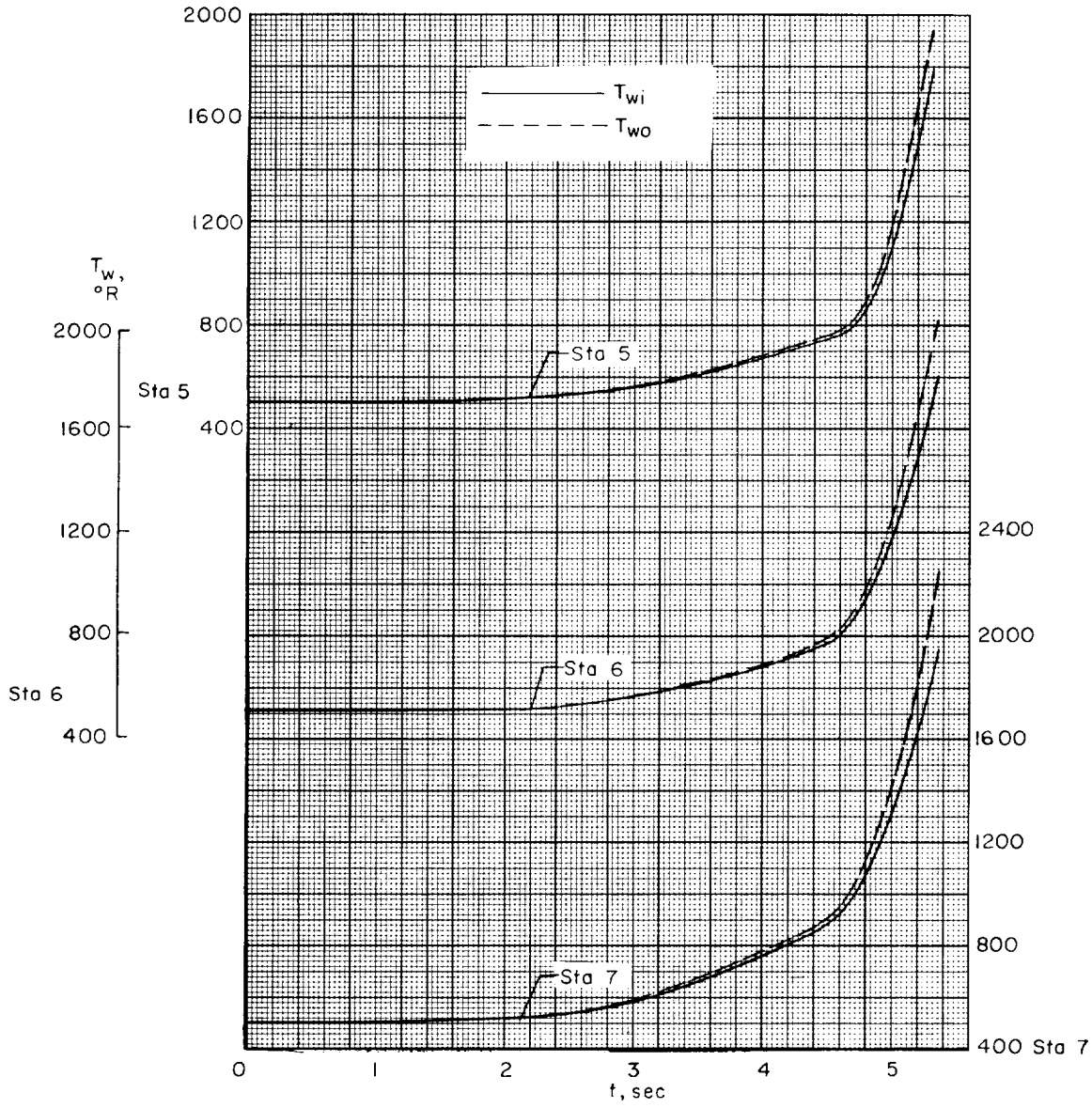

(b) Stations 5, 6, and 7.

Figure 7.- Concluded.

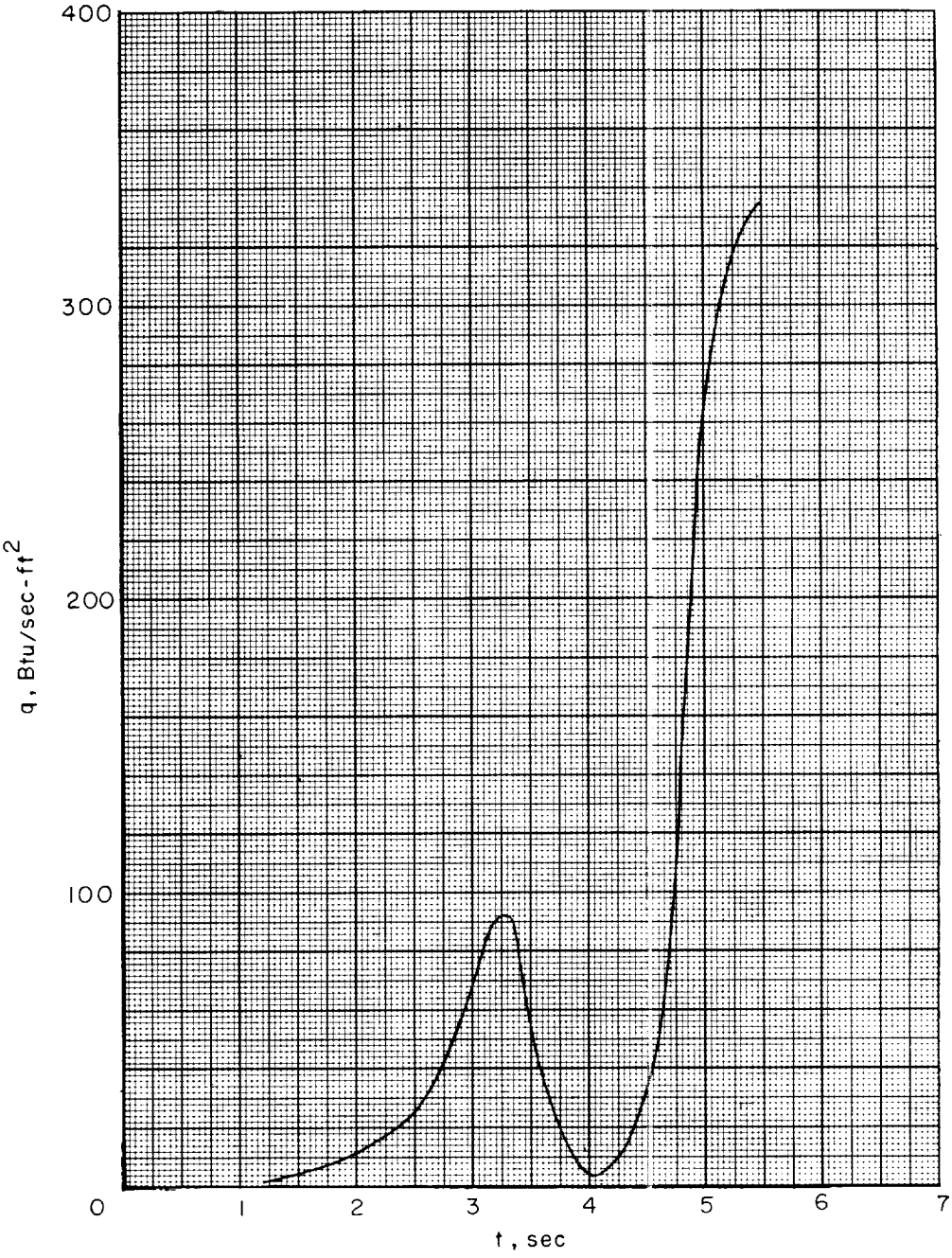

(a) Station 2.

Figure 8.- Typical variation of one-dimensional aerodynamic heating with flight time.

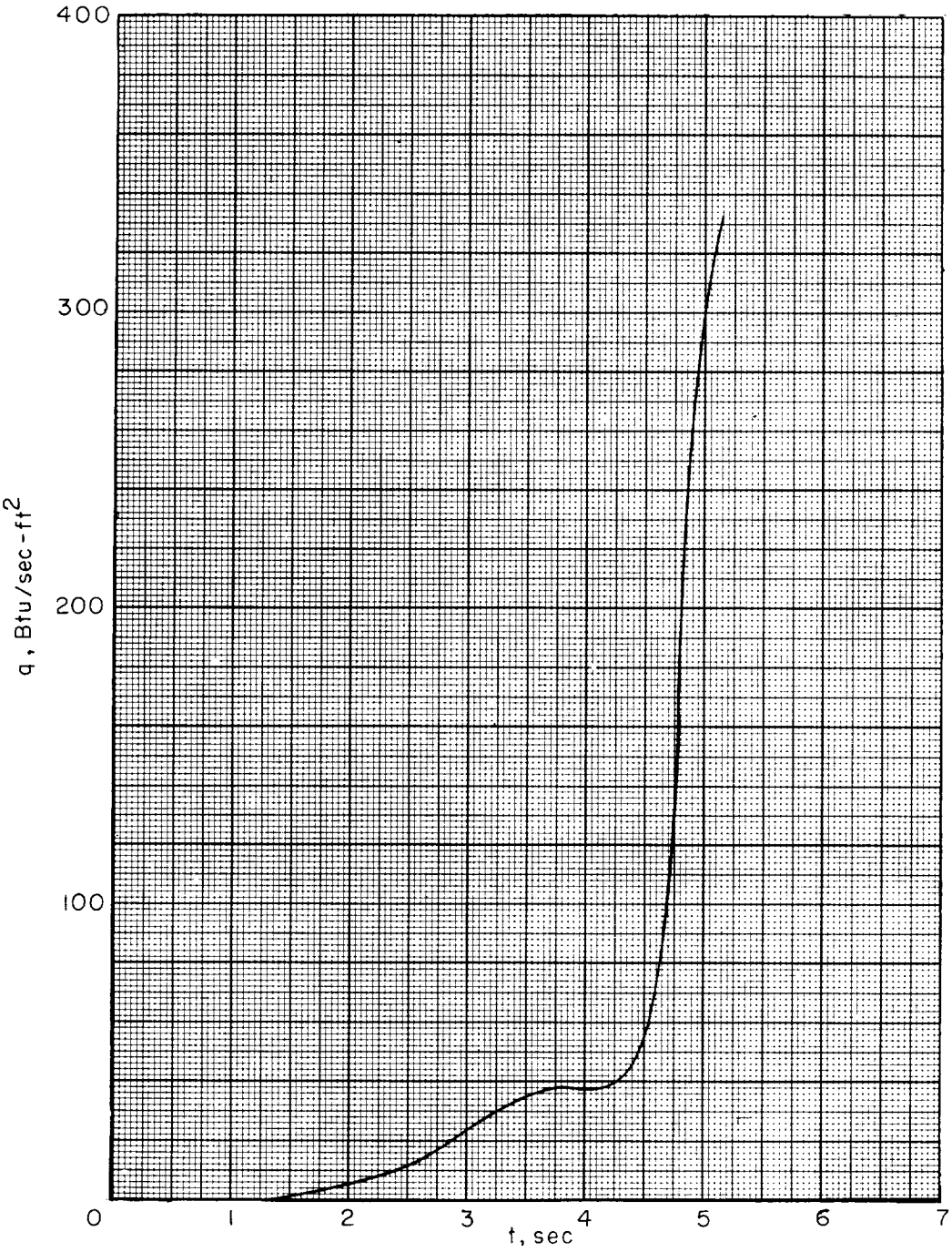

(b) Station 7.

Figure 8.- Concluded.

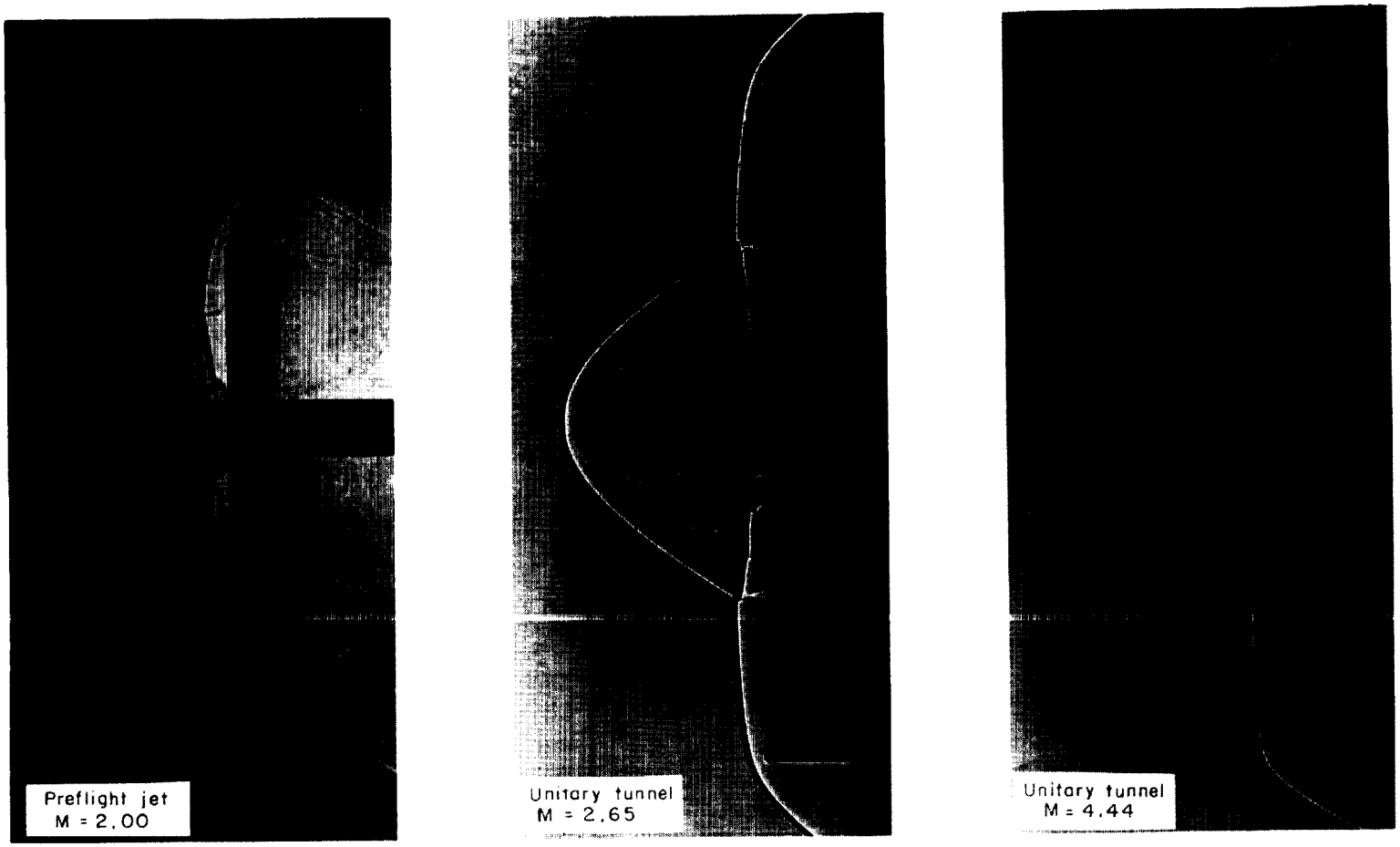

L-61-2242

Figure 9.- Shadowgraphs of typical shock patterns produced by a similar test configuration.

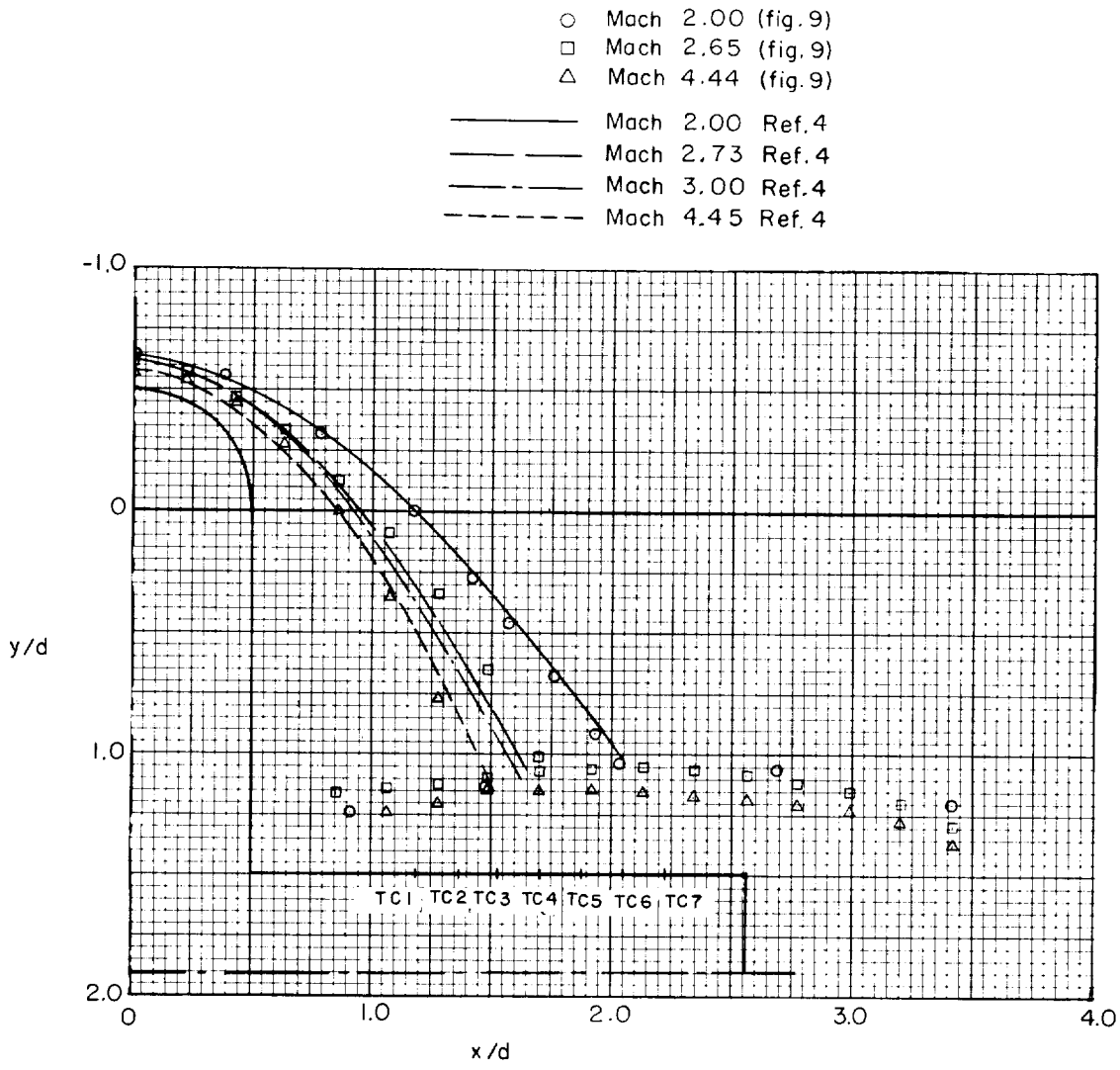

Figure 10.- Shock-wave geometry.

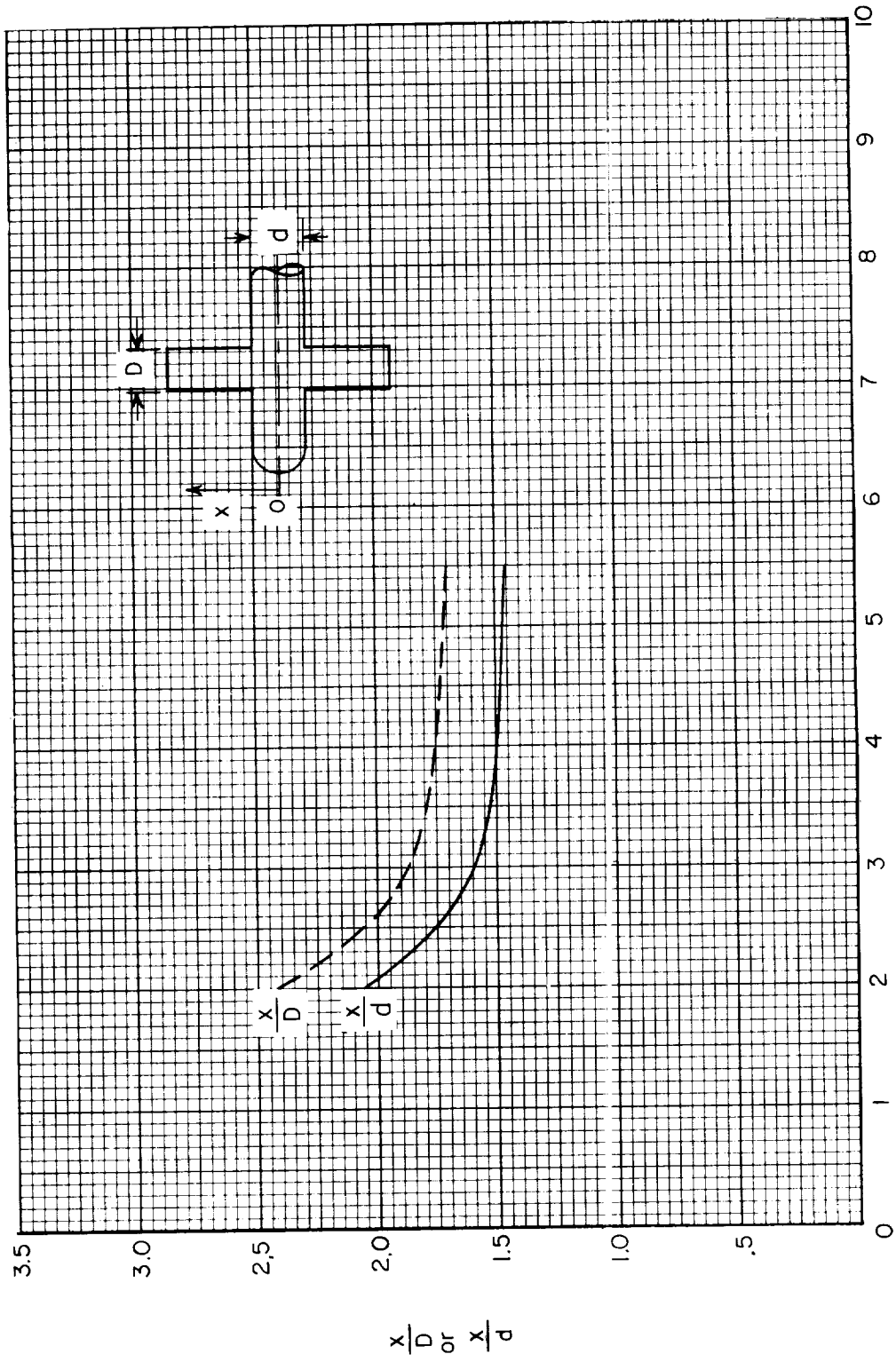

Figure 11.- Approximate location of shock intersection.

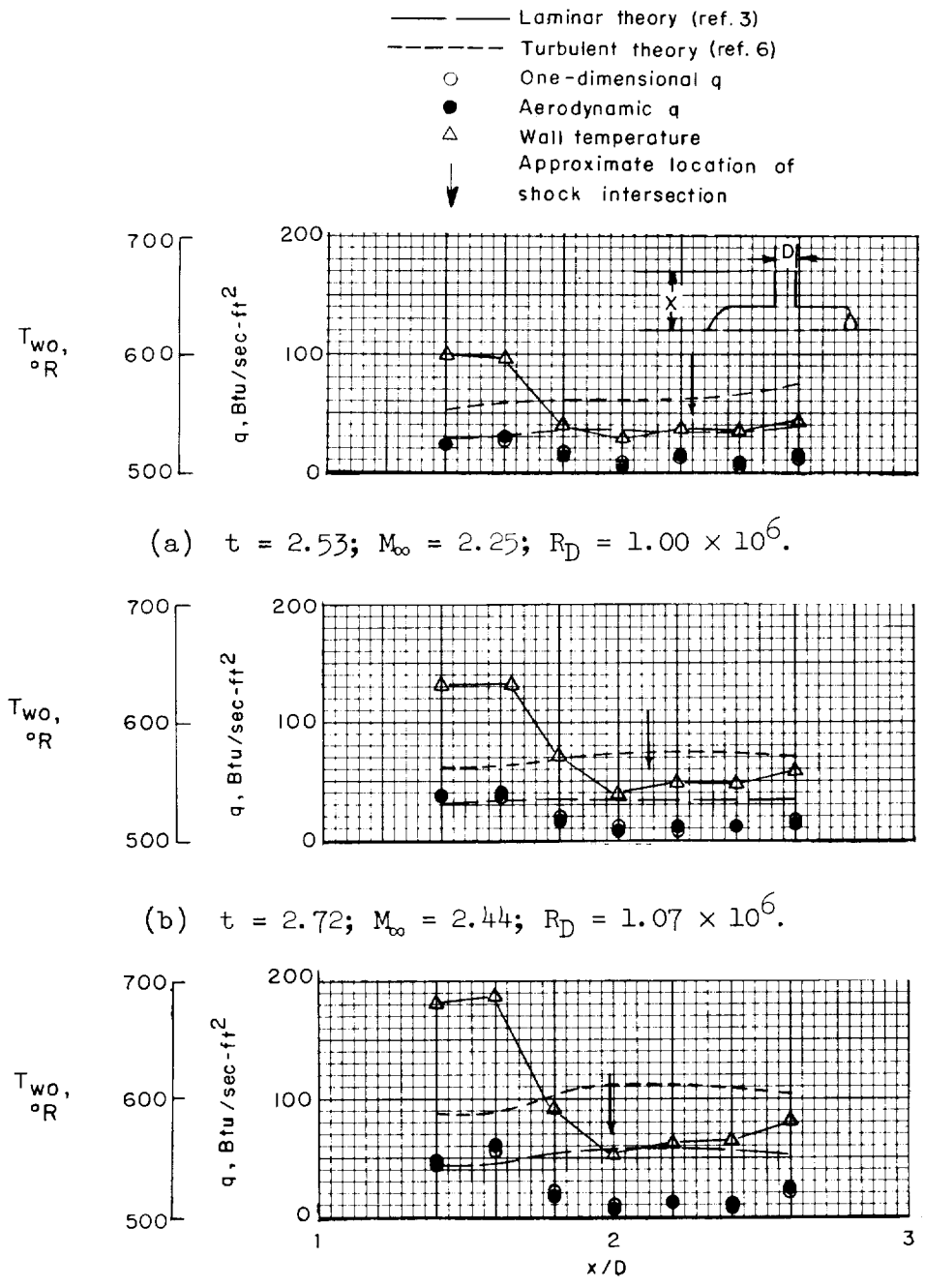

(a) $t = 2.53$; $M_\infty = 2.25$; $R_D = 1.00 \times 10^6$.

(b) $t = 2.72$; $M_\infty = 2.44$; $R_D = 1.07 \times 10^6$.

(c) $t = 2.91$; $M_\infty = 2.64$; $R_D = 1.13 \times 10^6$.

Figure 12.- Wall-temperature and heating-rate distributions at various flight conditions.

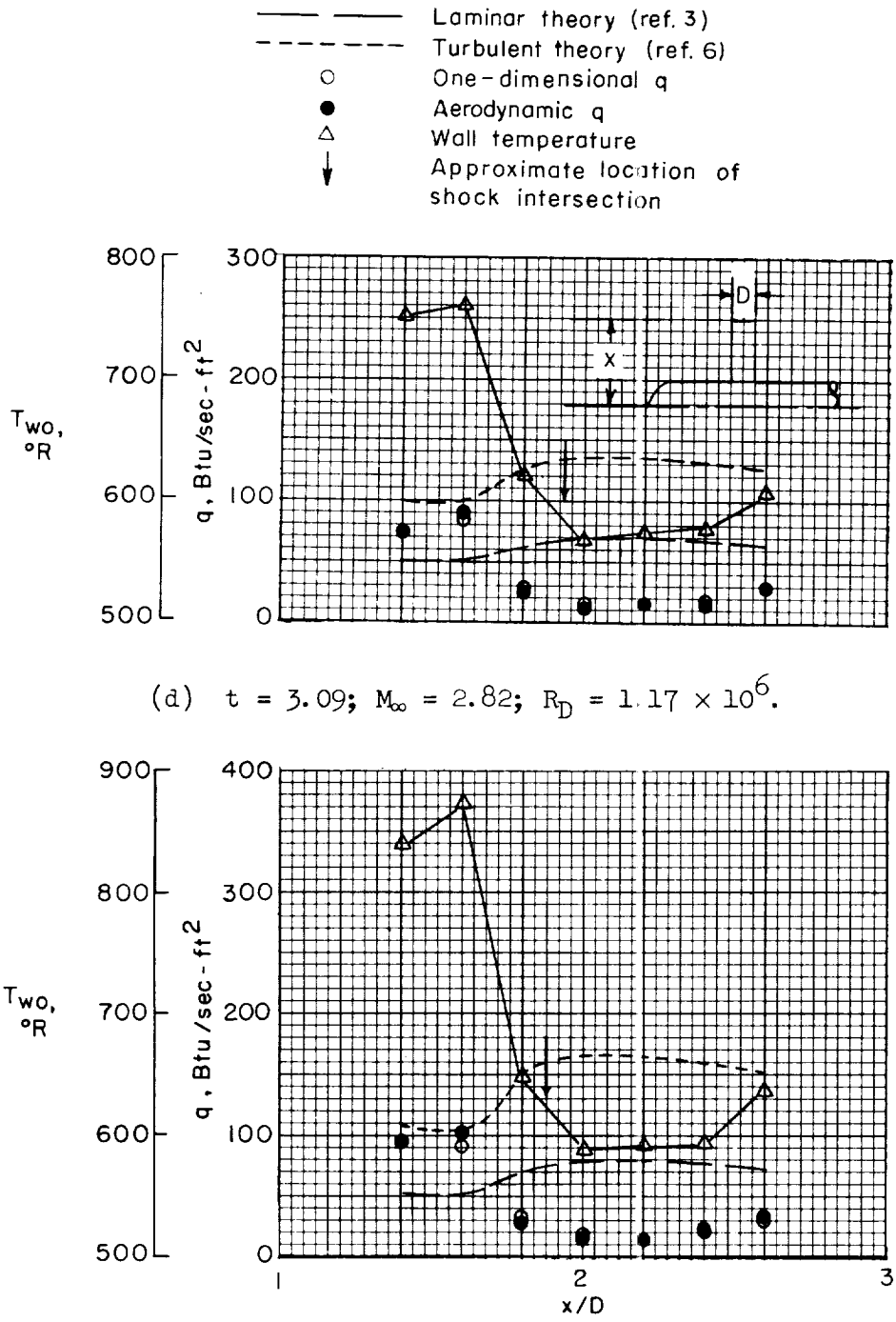

(d) $t = 3.09$; $M_\infty = 2.82$; $R_D = 1.17 \times 10^6$.

(e) $t = 3.28$; $M_\infty = 2.97$; $R_D = 1.22 \times 10^6$.

Figure 12.- Continued.

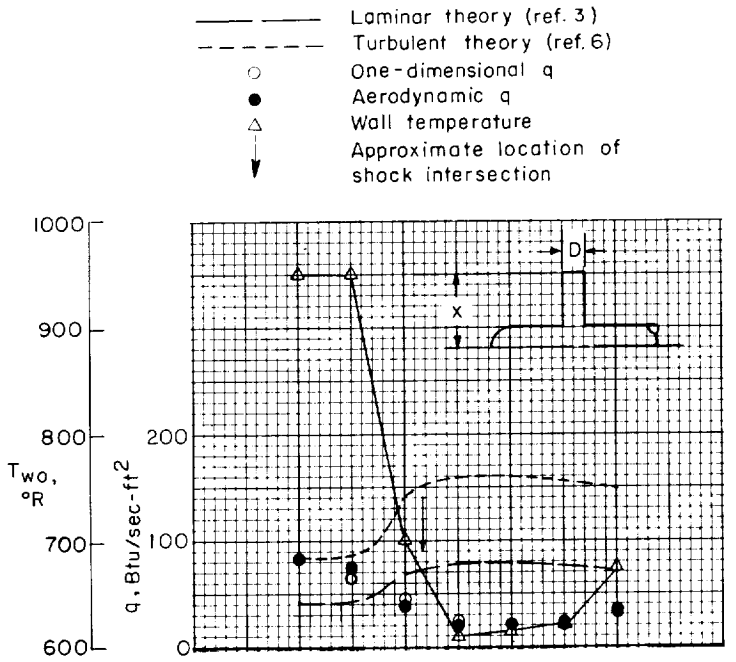

(f) t = 3.47; M_∞ = 3.00; R_D = 1.23 × 10^6.

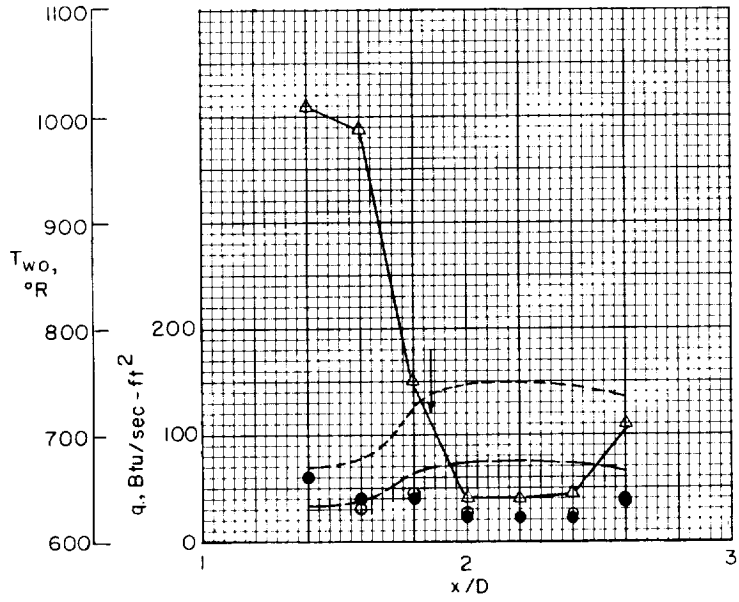

(g) t = 3.66; M_∞ = 3.00; R_D = 1.22 × 10^6.

Figure 12.- Continued.

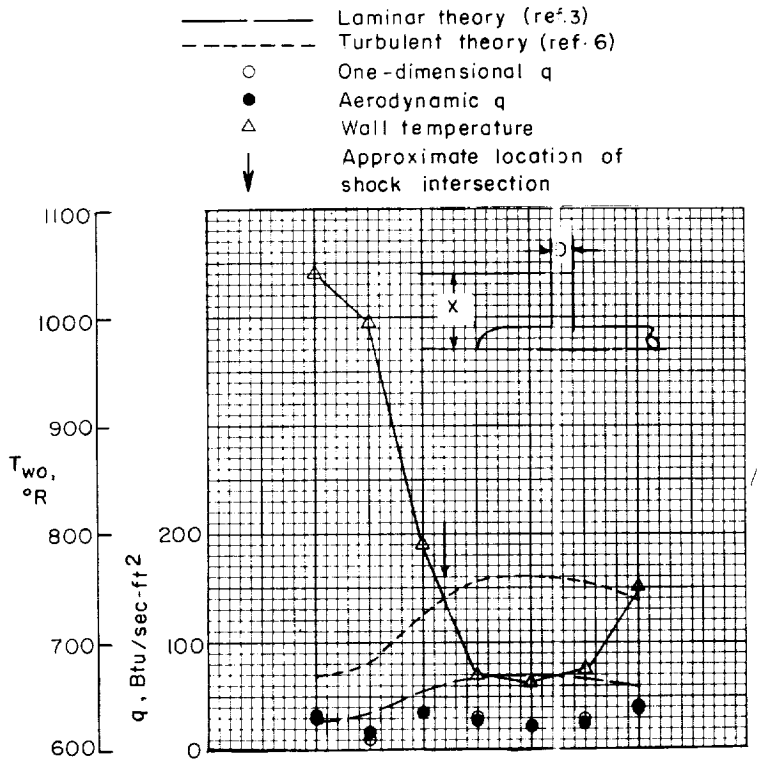

(h) $t = 3.84$; $M_\infty = 2.98$; $R_D = 1.19 \times 10^6$.

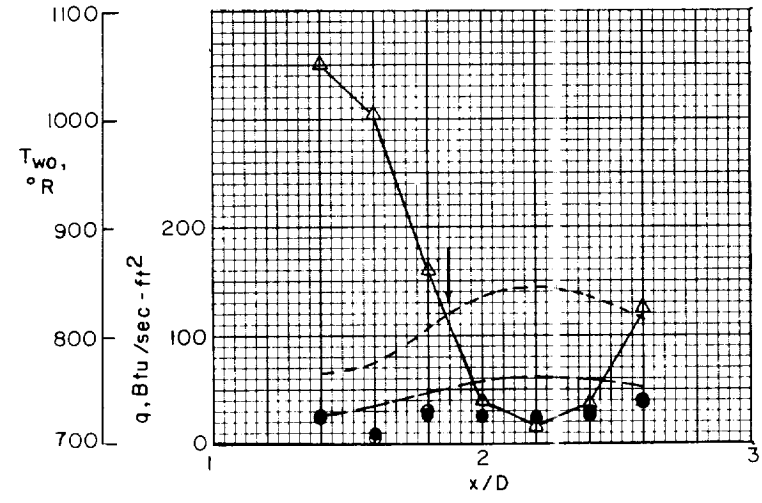

(i) $t = 4.03$; $M_\infty = 2.97$; $R_D = 1.15 \times 10^6$.

Figure 12.- Continued.

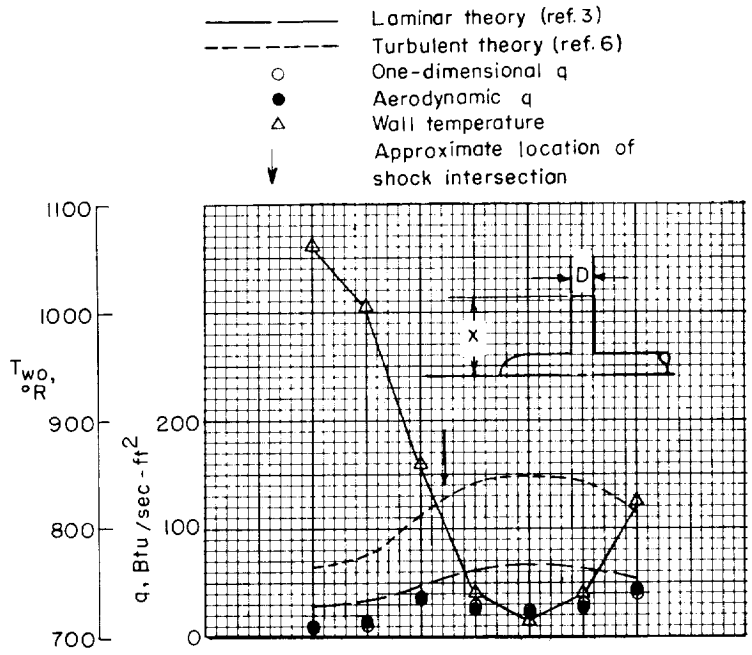

(j) t = 4.22; M_∞ = 2.95; R_D = 1.11 × 10^6.

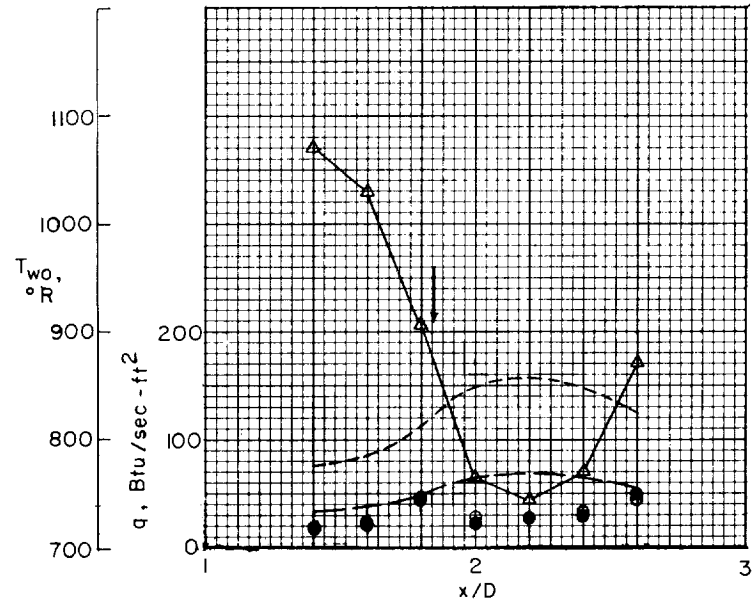

(k) t = 4.41; M_∞ = 3.04; R_D = 1.16 × 10^6.

Figure 12.- Continued.

Figure 12.- Continued.

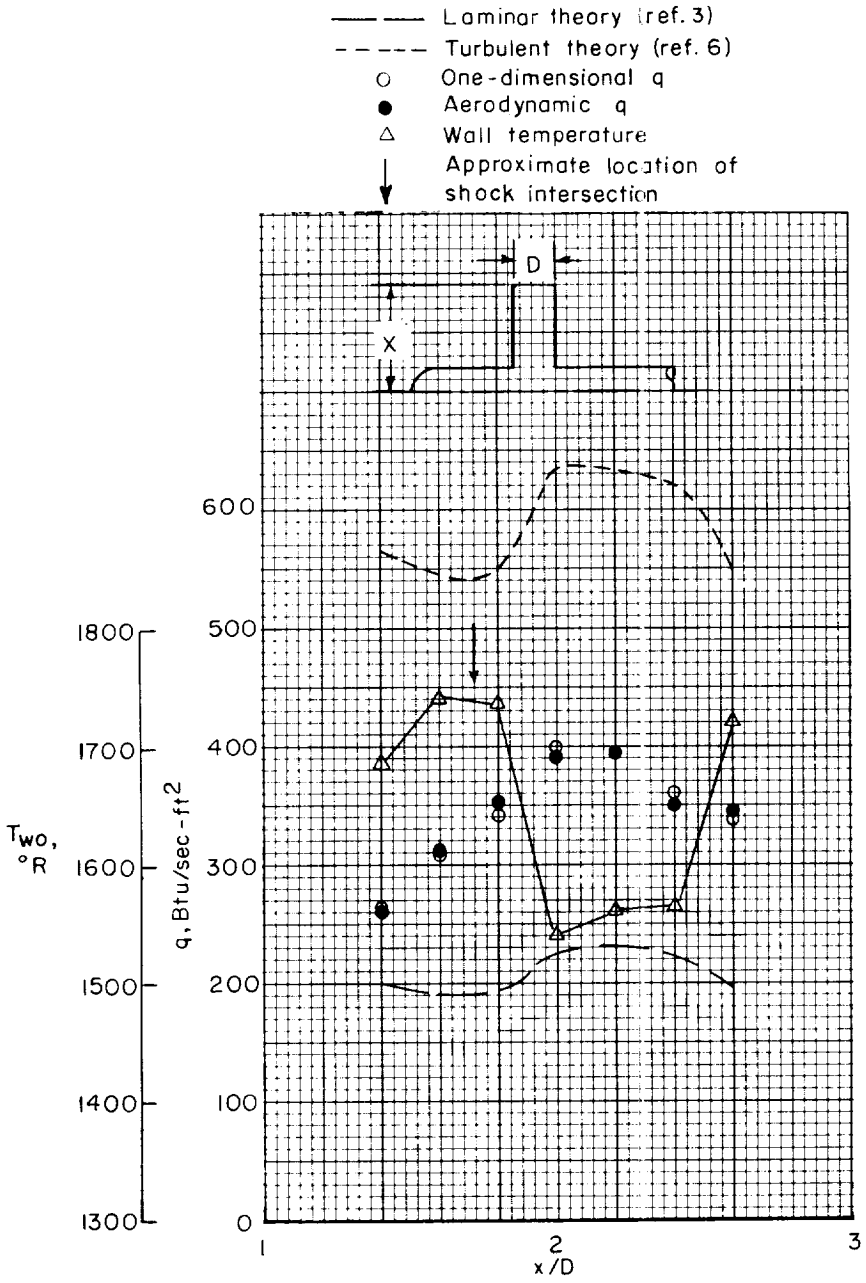

(o) $t = 5.16$; $M_\infty = 4.92$; $R_D = 1.71 \times 10^6$.

Figure 12.- Continued.

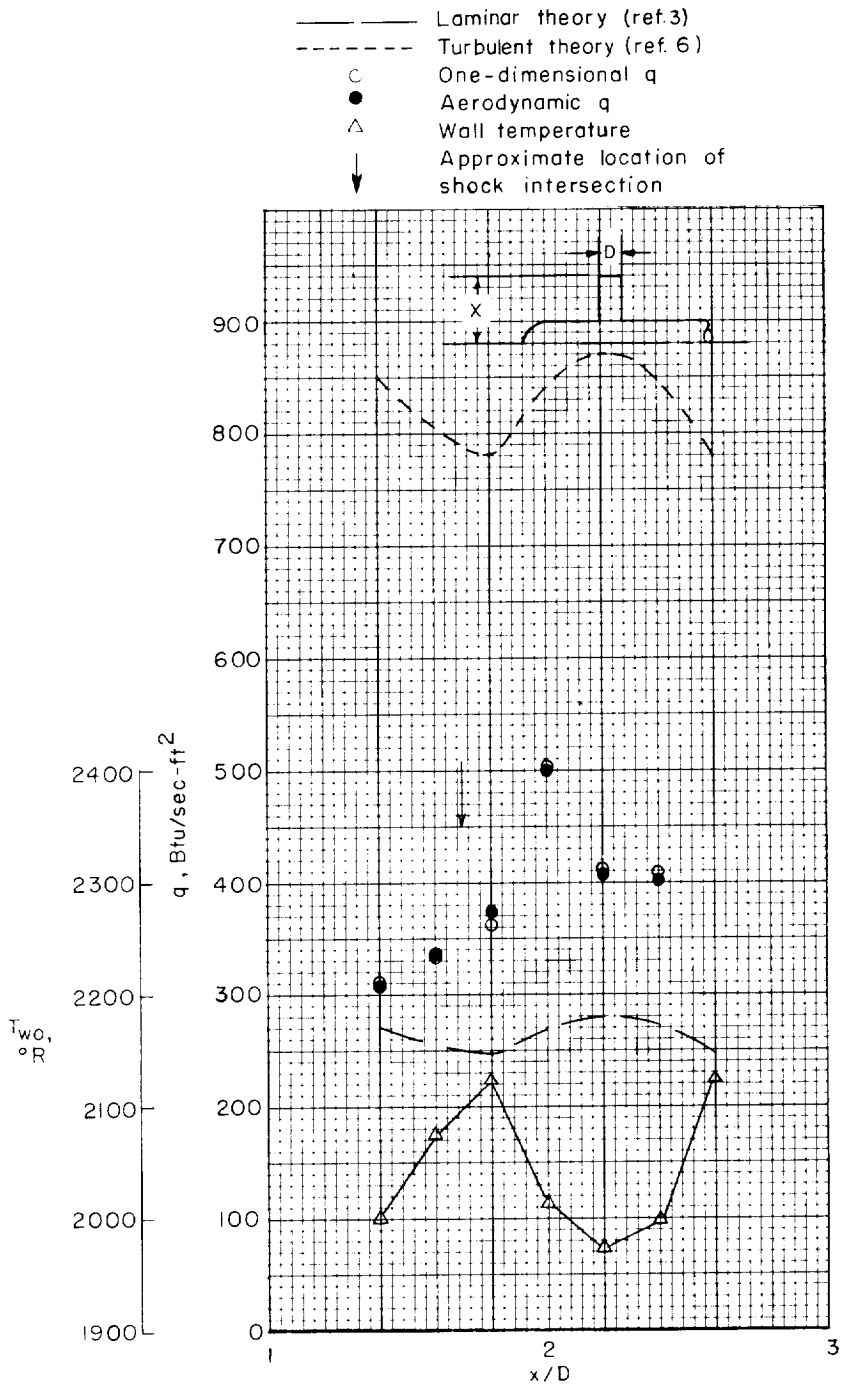

(p) $t = 5.34$; $M_\infty = 5.50$; $R_D = 1.87 \times 10^6$.

Figure 12.- Concluded.

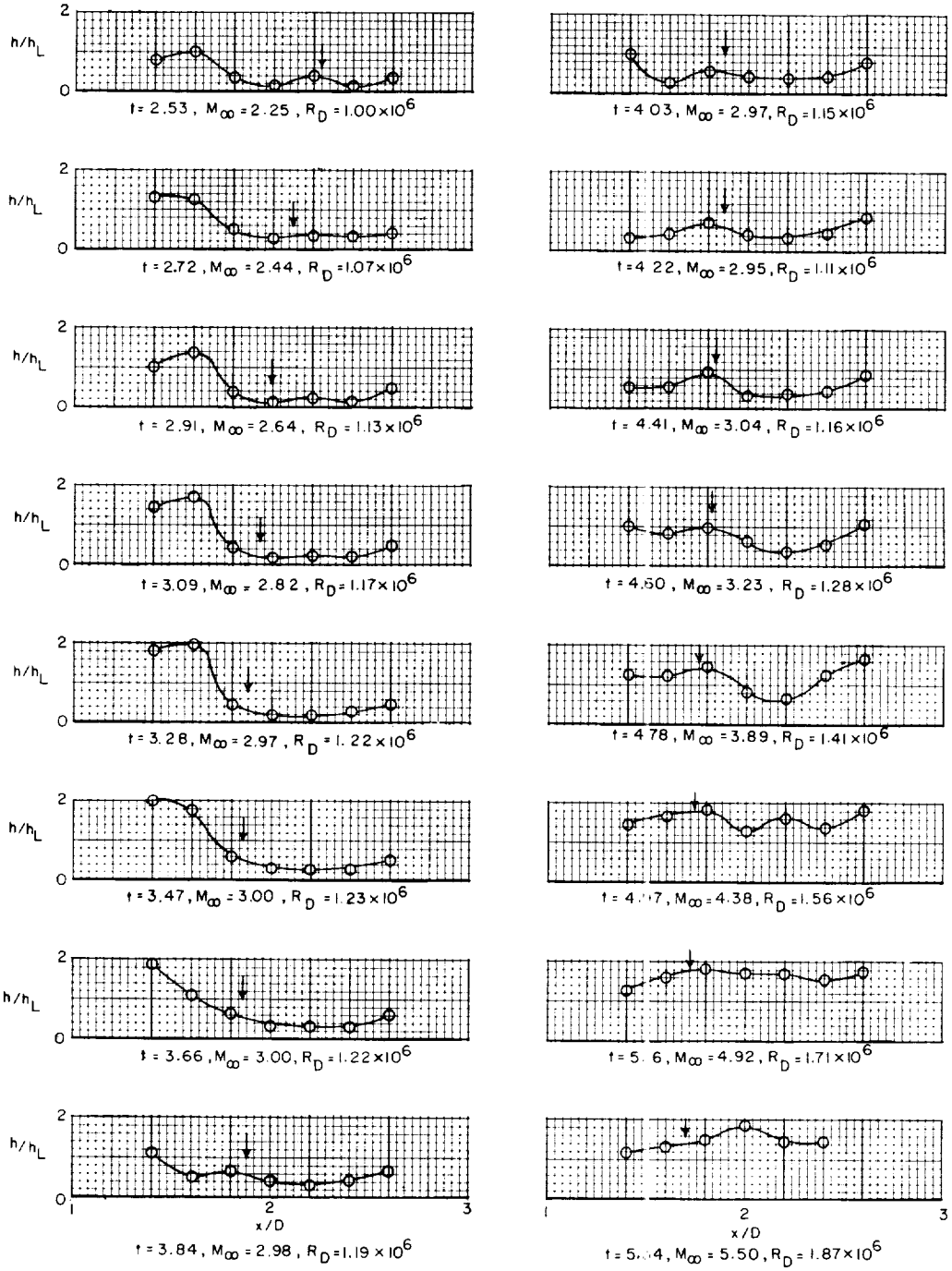

Figure 13.- Ratio of experimental heat-transfer coefficient to theoretical laminar heat-transfer coefficient for various flight conditions. Arrow indicates approximate location of shock intersection.

L-879